LANGMUIR

Invited Feature Article

Tools for Low-Dimensional Chemistry

Graham J. Leggett

Department of Chemistry, University of Sheffield, Brook Hill, Sheffield S3 7HF, U.K.

ABSTRACT: Many biological mechanisms can be considered to be low-dimensional systems: their function is determined by molecular objects of reduced dimensionality. Bacterial photosynthesis is a very good example: the photosynthetic pathway is contained within nano-objects (vesicles) whose function is determined by the numbers and nanoscale organization of membrane proteins and by the ratios of the different types of protein that they contain. Systems biology has provided computational models for studying these processes, but there is a need for experimental platforms with which to test their predictions. This Invited Feature Article reviews recent work on the development of tools for the reconstruction of membrane processes on solid surfaces. Photochemical methods provide a powerful, versatile means for the organization of molecules and membranes across length scales from the molecular to the macroscopic. Polymer brushes are highly effective supports for model membranes and versatile functional and structural components in low-dimensional systems. The incorporation of plasmonic elements facilitates enhanced measurement of spectroscopic properties and provides an additional design strategy via the exploitation of quantum optical phenomena. A low-dimensional system that incorporates functional transmembrane proteins and a mechanism for the in situ measurement of proton transport is described.
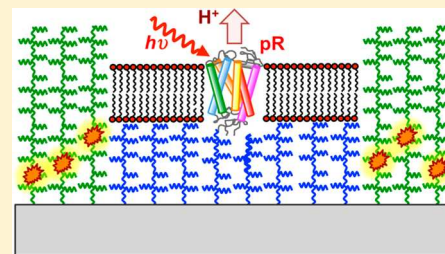
INTRODUCTION

In physics, low-dimensional structures are ones whose reduced dimensions cause them to exhibit new or modified properties when compared to bulk phases of matter. For example, the band structure of a quantum dot is different from that of a bulk semiconductor made of the same material as a consequence of the confinement of the electronic wave function and may be adjusted simply by changing the dimensions of the object.

There is an important sense in which one might also argue that many biological systems exhibit special characteristics that are a consequence of their having reduced dimensionality. These properties do not result from quantum confinement, however. Membranes have a critical role in controlling cellular function and provide important illustrations of low-dimensional molecular systems. For example, they contain sensing elements, pumps, channels, and synthetic apparatus. Cellular membranes are two-dimensional structures, and the dimensional confinement of their constituent components is necessary for their function. For example, the conversion of ADP to ATP by ATP synthase is driven by a one-dimensional transmembrane proton gradient. Indeed, the fact that single-molecule experiments have become such an important part of biological science is an acknowledgment of the importance of reduced dimensionality in biology: single-molecule experiments have changed the way that many biological problems are viewed because they provide the means to avoid ensemble averaging. However, there is a deeper sense in which biological systems may be said to be low-dimensional.

In purple bacteria, the photosynthetic apparatus is contained in chromatophore vesicles (Figure 1).[1] Light energy is captured by light-harvesting complex 2 (LH2), where it is transferred internally via a series of steps to the lowest-energy state (Q_y) of

the B850 ring of 18 bacteriochlorins. From here the excitation is transferred from complex to complex via a series of Förster resonance energy transfer (FRET) steps before it reaches the light-harvesting complex 1/reaction center (LH1/RC) complex where charge separation occurs. Electron transfer to a quinone results, yielding a quinol which diffuses through the vesicular membrane until it reaches the cytochrome bc_1 complex to be oxidized to a quinone, driving proton transfer across the membrane. The resultant transmembrane proton gradient drives the conversion of ADP to ATP by ATP synthase. Figure 1a shows a computational model of the chromatophore vesicle for *Rhodobacter sphaeroides* constructed using a combination of data from atomic force microscopy (AFM), electron microscopy, crystallography, and spectroscopy.[2] Shown alongside the model (Figure 1b) is an AFM image of an intact chromatophore vesicle[3]—the first AFM image of an intact spherical organelle—confirming the validity of the model.

The chromatophore vesicle can be considered to be a low-dimensional system. First, it is small, a little larger than a single transistor in a modern integrated circuit yet containing an entire biochemical pathway rather than merely a bit of information. Second, its function is determined by its reduced dimensionality. Each vesicle contains on average 2 ATP synthase molecules, for example,[2] and the function of the vesicle is determined by the ratios of the other protein components. Under low light conditions, there are 2.7 LH2 complexes for each LH1/RC complex and 3 LH1/RC complexes for each cytochrome bc_1 dimer.[2] It is evident that besides control of the stoichiometry of the vesicle
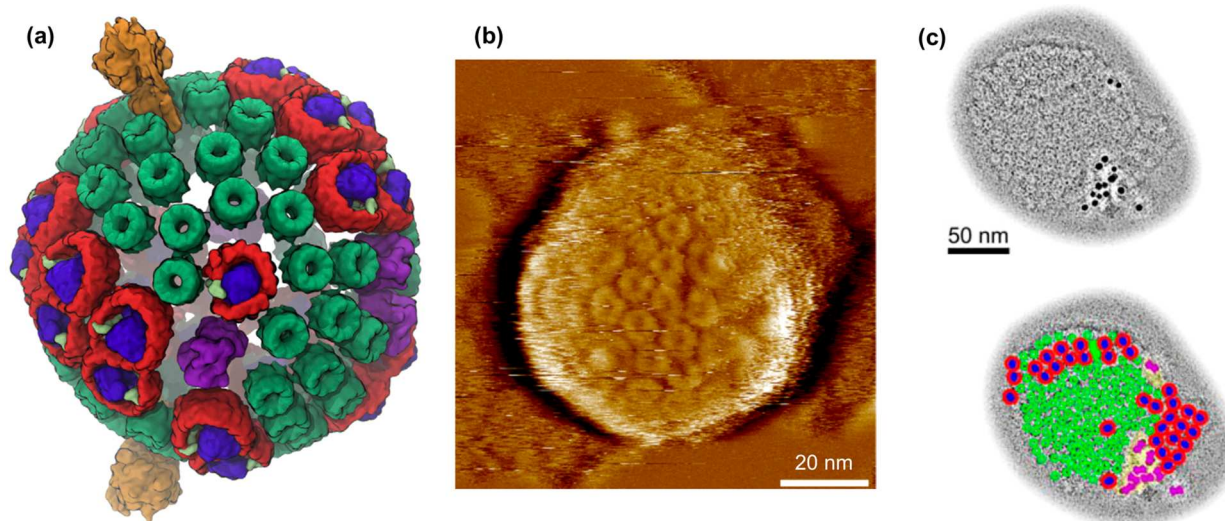
Figure 1. (a) Atomic-level model of the chromatophore vesicle from *R. sphaeroides*. (b) Atomic force microscopy image of an intact chromatophore vesicle. (c) Electron micrograph of a flattened vesicle unmodified (top) and with color-coded membrane proteins (bottom). (a and c) LH2 = green, LH1 red, RC = blue, cytochrome bc_1 = magenta, and ATP synthase = brown. (a and c) Reproduced with permission from ref 2, copyright 2014 Elsevier. (b) Reproduced from ref 3, copyright 2017 American Chemical Society.

there is also a degree of spatial organization. For example, the cytochrome bc_1 complexes (magenta) are clustered together, while the LH2 antenna complexes (green) form a band several tens of nanometers wide. The width of this band is probably important because after the capture of a photon, excitonic transport via FRET will occur with a characteristic, finite diffusion length. It is thus clear that in important ways these functional biological nanosystems can be thought of as being low-dimensional systems.

LOW-DIMENSIONAL MOLECULAR SYSTEMS

It has been a long-standing goal in my laboratory to develop platforms that enable low-dimensional systems and, in particular, photosynthetic pathways, to be examined experimentally. Computationally, they can be investigated using a systems biology approach[4]—the pathway can be represented as a series of discrete units connected via inputs and outputs, each of which can be modeled. Cartron et al. constructed an atomic-level model of a chromatophore vesicle[2] and were able to model the interconnected energy-, electron-, and proton-transfer processes involved in the capture of sunlight and its conversion to ATP, stored chemical potential energy (Figure 2a). Significantly, while the quantum efficiencies of the light-harvesting proteins in purple bacterial are thought to approach 100%, a half-maximal ATP turnover rate was found for a light intensity equivalent to only 1% of bright sunlight.[2] This result illustrates one of the intriguing challenges in biologically inspired design: while we can discover in nature functional structures and systems that suggest models for the design of new materials and devices to serve anthropomorphic ends, we must beware of the mindless copying of biological systems because they have evolved to serve different functions. Purple bacteria are adapted by evolution to survive and multiply under conditions where light levels are low.

An alternative approach to studying biological systems is to make adaptations to natural ones. Grayson et al. produced a strain of *R. sphaeroides* in which the reaction centers were modified by the attachment of yellow fluorescent protein (YFP).[5] Fluorescence lifetime measurements confirmed that there was spectral overlap between the emission of YFP and the visible-region (Q_x)

absorption bands of the RC. This facilitated energy transfer via FRET, leading to an enhanced rate of growth in cultures of the bacteria (Figure 2b).

However, it is useful to be able to ask fundamental questions that may require an experimental approach that is not tied to structures found in biology. Figure 2c shows a design concept for a low-dimensional molecular system. Although the basic architecture of such a system is simple, it presents substantial fabrication challenges. It consists of a membrane protein that is located within a supported lipid bilayer (SLB) that serves as a model for the cellular membrane. The membrane must be raised above the solid surface on which it is supported because membrane proteins typically extend some distance on either side of it. The device must also contain a region that is a surrogate for the interior of the vesicle or cell to enable transmembrane transport to be measured. Compartmentalization is desirable because it assists in the accumulation of a transmembrane gradient and may facilitate the measurement process. Finally, a mechanism is required to monitor the function of the membrane protein and/or any transmembrane transport processes.

Such a system is easy to represent schematically but challenging to build. The remainder of this Invited Feature Article describes progress toward the development of the tools required to construct functional systems such as the one shown in Figure 2c. We find that a combination of photochemistry and polymer brush synthesis is extremely powerful.

ORGANIZATION OF PROTEINS ON THE NANOMETER SCALE

The first requirement for the organization of proteins on surfaces is the existence of effective mechanisms for the control of nonspecific adsorption; the function of the patterning is to introduce protein-binding regions at selected locations in the biologically inert background. The most widely used approaches to the inhibition of protein adsorption have been based on poly(ethylene glycol) and its derivatives.[6−11] However, a number of other polymers have been found to provide resistance to protein adsorption, including poly(sulfo betaines)[12,13] and
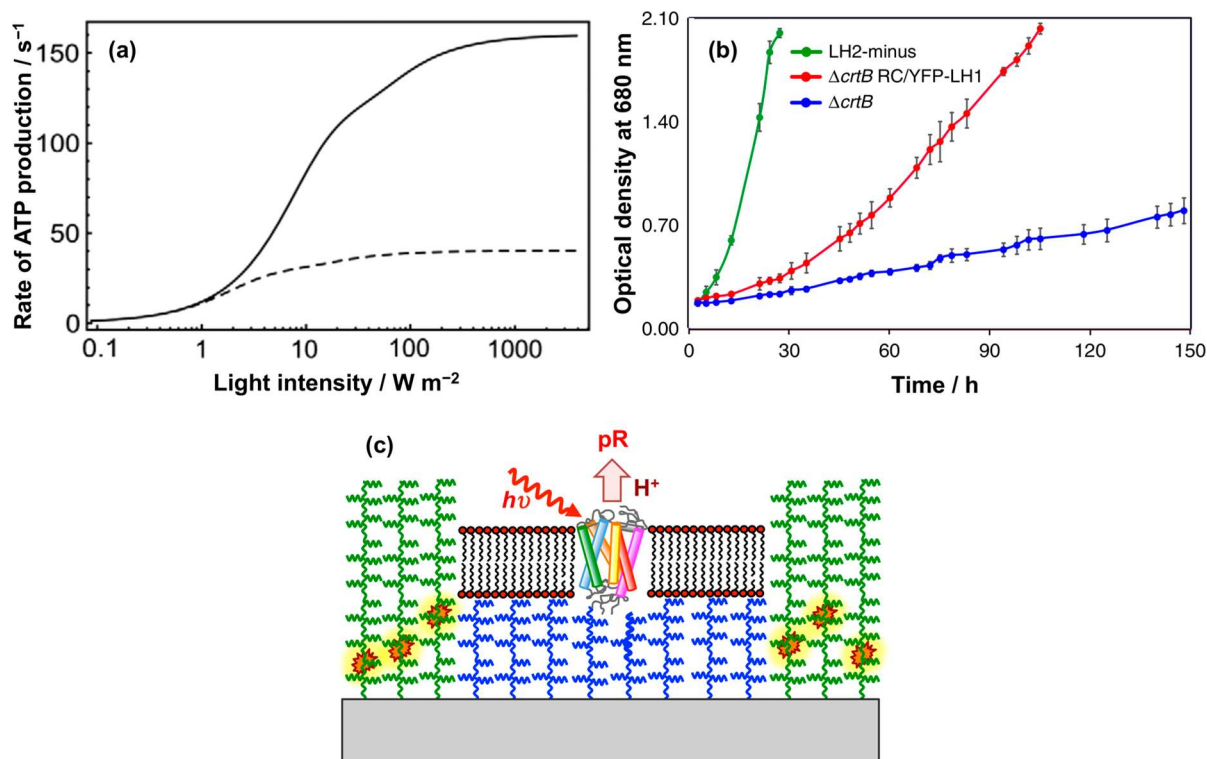
Figure 2. Biological systems. (a) ATP production rate as a function of incident light intensity for the chromatophore vesicle from *R. sphaeroides*. The dashed line shows the effect of reducing the number of cytochrome bc_1 complexes from 4 to 1 while increasing the number of LH2 units by 7. (b) Photosynthetic growth curves for strains of bacteria with carotenoid-free LH1 with (red) and without (blue) the addition of YFP. The green line shows data for a carotenoid-containing LH2 minus strain as a control. (c) A conceptual design for a low-dimensional system in which a membrane "corral" is formed consisting of a supported lipid bilayer (SLB) resting on a polymer brush cushion and surrounded by polymer brush walls that incorporate optical reporters. (a and b) Reproduced with permission from ref 5, copyright 2017 Nature Publishing Group.

zwitterionic polymers such as poly(2-(methacryloyloxy)ethyl phosphorylcholine).[14,15]

Inspired by the concept of light-directed chemical synthesis,[16] the use of lithographic exposure in conjunction with photo-removable protecting groups to conduct spatially selective solid-phase synthesis, we have developed aminosilanes with photo-removable, protein-resistant protecting groups that enable the spatially selective conversion of a protein-resistant surface to a protein-binding one.[17] In particular, an aminosilane bearing a photoremovable nitrophenyl group derivatized with an oligo-(ethylene glycol) adduct, (methoxyheptaethylene glycol)nitro-phenylethoxycarbonyl-protected aminopropyltriethoxysilane (henceforth OEG-NPEOC-APTES),[17,18] has proved to be a versatile tool for the patterning of proteins at surfaces. After deprotection of the aminosilane, either through a mask or using a scanning near-field optical microscope, the amine terminal groups are derivatized first with glutaraldehyde and then with *N*-(5-amino-1-carboxy-pentyl)iminodiacetic acid to yield a nitrilo triacetic acid (NTA)-terminated surface.[19] After complexation with Ni^{2+}, this surface binds histidine-tagged proteins in a site-specific fashion.

The efficacy of this simple system was demonstrated in studies of the patterning of His-tagged green fluorescent protein (GFP) (Figure 3a).[18] We formed patterns of His-GFP and then treated them with imidazole to disrupt the protein–surface interaction (Figure 3b). The contrast between regions that were masked and exposed during photopatterning was compared quantitatively using line sections through raw, unfiltered images (Figure 3c,d). Regions of the surface not exposed to UV light bound negligible amounts of His-tagged proteins, indicating that the oligo(ethylene glycol) adduct on the nitrophenyl protecting

group confers excellent protein resistance. In contrast, exposed regions bound His-GFP very effectively, yielding strong fluorescence that was almost completely removed on treatment of the surface with imidazole, confirming a degree of site-specific binding in excess of 90%.

Near-field methods are effective for the patterning of molecular films on the nanometer scale.[20] Films of OEG-NPEOC-APTES can be patterned by near-field exposure at 325 nm (Figure 3e),[21] enabling selective removal of the protein-resistant protecting group and functionalization with biotin or NTA functional groups to enable site-specific binding of, respectively, neutravidin-coated polymer nanoparticles[17] and His-tagged GFP.[18] Films of organic adsorbates may also be patterned photo-catalytically on the nanoscale by coating a near-field probe with a thin film of titania and using the near field to excite highly localized oxidative degradation of organic matter. In this way, it is possible to pattern protein-resistant oligo(ethylene glycol) groups, enabling site-specific binding of His-tagged proteins (Figure 3f).[22]

For many years the development of methods for the fabrication of multiple-component protein nanopatterns remained challenging. Maynard and co-workers have achieved the most impressive results to date.[23,24] Using electron beam lithography, they patterned biotin, maleimide, aminoxy, and nitrilotriacetic acid groups onto protein-resistant surfaces, using them to bind proteins that incorporated complementary affinity tags.[23] However, a limitation of such an approach is that there is a finite range of suitable affinity tags.

Recently we demonstrated the efficacy of a simple alternative approach based on the near-field exposure of OEG-NPEOC-APTES films.[21] A pattern was first fabricated by near-field
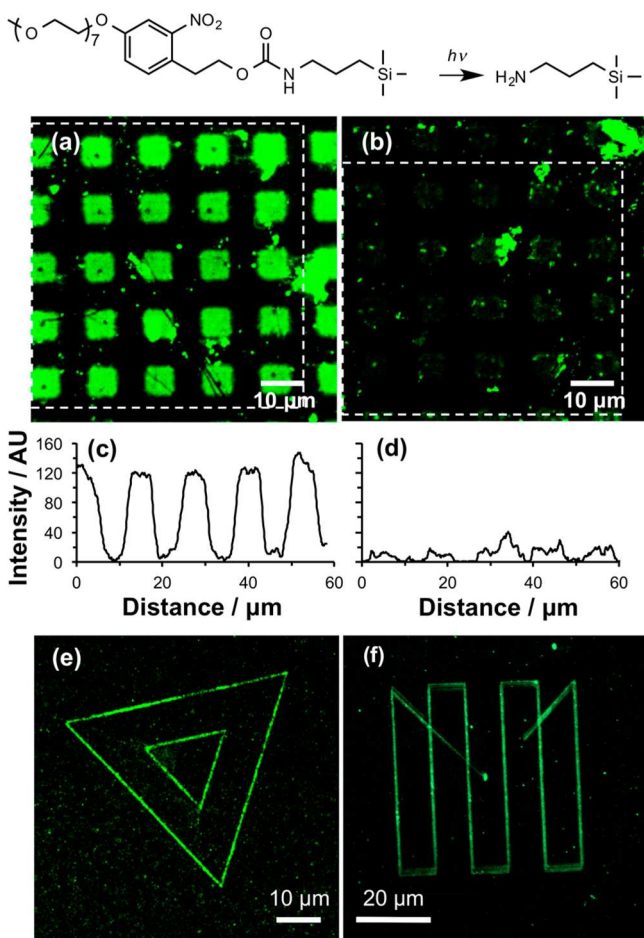
Figure 3. Fluorescence microscopy of protein patterns. (a) Pattern formed by exposure of an OEG-NPEOC-APTES film to near-UV light through a mask, derivatization with NTA, complexation with Ni^{2+}, and immersion in a solution of His-GFP. (b) The sample shown in panel a after treatment with imidazole to disrupt the His-NTA interaction. (c and d) Sections through the regions identified by dashed boxes in panels a and b, respectively. (e) Nanopattern formed by using near-field exposure followed by the adsorption of FITC-labeled IgG. (f) His-GFP nanopattern formed by photocatalytic nanolithography followed by the conjugation of NTA to modified regions, complexation to Ni^{2+}, and immersion of the sample in a solution of the protein. (a−d) Reproduced from ref 18, copyright 2016 American Chemical Society. (e) Reproduced from ref 21, copyright 2017 American Chemical Society. (f) Reproduced from ref 22, copyright 2013 American Chemical Society.

exposure of the unmodified film, causing localized removal of the protein-resistant protecting group. Immersion of the sample in a solution of a protein with a fluorescent dye yielded a protein nanopattern via physisorption of the protein onto the solid surface that could be visualized using confocal microscopy. The sample was then returned to the near-field microscope to write additional structures. Figure 4 shows patterns formed on a single substrate by the serial execution of four lithographic steps. In each step, a protein containing a different fluorescent label was adsorbed onto the surface. The effectiveness of the patterning methodology is demonstrated clearly. Key to the success of this multistep process is the use of a highly protein-resistant background material capable of being used in multiple, repeated adsorption steps without significant adsorption of proteins in areas unmodified by the lithographic steps.

■ A FAST, SIMPLE ROUTE TO LARGE-AREA NANOFABRICATION

To address many problems in biology it is useful to be able to fabricate nanostructures over macroscopically extended areas. One way of achieving this using photolithography is to use a parallel near-field lithography system, such as the "Snomipede", in which light is delivered to an array of separately actuated near-field probes.[25] Another approach is to use interferometric lithography[26,27] in which two or more coherent laser beams interfere to produce an interferogram (a pattern of alternating bands of constructive and destructive interference) with a sinusoidal cross section of pitch $\lambda/2n \sin \theta$, where λ is the wavelength, n is the refractive index of the medium, and 2θ is the angle between the interfering beams. The interferogram covers an area of ∼1 cm^2 in the apparatus used in the author's laboratory but the method is in principle scalable to enable the processing of larger areas. While it does not permit arbitrary pattern formation, as near-field methods do, IL offers the important advantages that it is fast and uses simple apparatus.

Interferometric exposure of OEG-NPEOC-APTES films enables the fabrication of two-component patterns over cm^2 regions.[21] Exposure of a self-assembled monolayer (SAM) of alkylphosphonates on a photocatalytically active titania surface to UV light causes localized photodegradation of the adsorbates, creating a nanopatterned SAM that can be used as a resist for the selective etching of exposed regions of titania.[28] Structures with a full width at half-maximum (fwhm) of as small as 25 nm can be formed. Figure 5a shows a titania nanostructure formed in this way but with a larger pitch to enable imaging by confocal microscopy after the adsorption of proteins. The surface is then rendered protein-resistant by the adsorption of an OEG-terminated silane and subsequently exposed to near-UV light to cause the photocatalytic removal of the protein-resistant adsorbates from the titania regions. However, they are left intact on the silica regions between the nanostructures. This enables protein adsorption onto the titania, while the silica regions between them remain protein-resistant. Figure 5c shows a confocal fluorescence microscopy image of GFP adsorbed to titania nanostructures formed by IL. Flooding the surface with near-UV light causes the photocatalytic removal of the protein, regenerating clean titania nanostructures that can be coated with a monolayer of a different protein, for example, yellow fluorescent protein (YFP) as shown in Figure 5d.

Plasmonic nanoparticles are attractive as functional elements in low-dimensional systems because they can be used to enhance the intensities of optical transitions in single biological molecules, thus facilitating spectroscopic analysis. Arrays of plasmonic nanostructures may be fabricated by using IL to expose alkylthiolate SAMs adsorbed on gold films.[29] Because of the simplicity and versatility of IL, a wide range of morphologies can be fabricated over macroscopic areas by simply varying the angle between the interfering beams and the angle of rotation between exposures.

When proteins are attached to plasmonic nanoparticles, a small red shift is observed in the position of the plasmon band, attributed to a local modification of the refractive index by adsorption of the biomolecule onto the nanoparticle surface.[30] However, when wild-type (WT) LH2 from *R. sphaeroides* is adsorbed onto arrays of gold nanostructures, a very different type of behavior is observed (Figure 6a).[31] The plasmon band is split, a phenomenon attributed to strong plasmon−exciton coupling,[32−35] leading to the creation of new "plexitonic" states above and below the energy of the localized surface plasmon
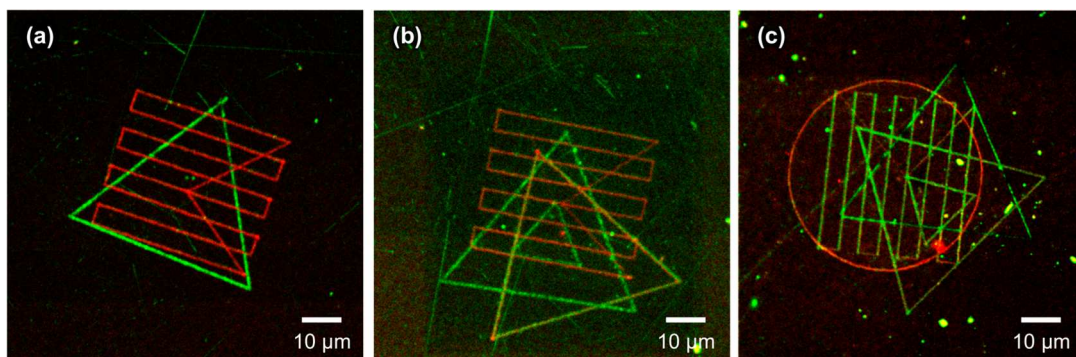
Figure 4. Stepwise assembly of multiple-component protein nanopatterns using near-field lithography.[21] (a) GFP + streptavidin-Atto 655. (b) IgG-FITC + streptavidin-Atto 655 + streptavidin-Atto 488. (c) IgG-FITC + streptavidin-Atto 655 + streptavidin-Alexa Fluor 488 + streptavidin-Alexa Fluor 750. A representative line section is provided beneath each micrograph, measured between the white arrowheads marked on each. Reproduced from ref 21, copyright 2017 American Chemical Society.
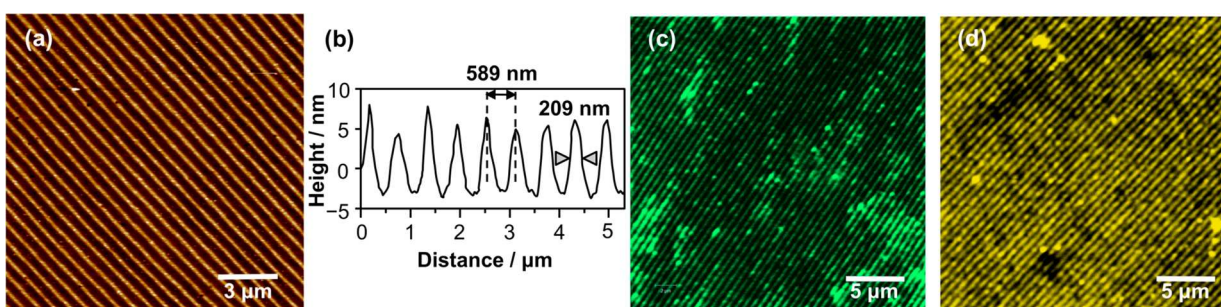
Figure 5. (a) Tapping-mode AFM height image of TiO_2 nanostructures fabricated for protein nanopatterning experiments. (b) Line section showing a period of 589 nm and fwhm of 209 nm. (c) Confocal fluorescence micrograph after the adsorption of GFP onto the sample shown in panel a. (d) Fluorescence micrograph of the sample shown in panel c after photocatalytic cleaning of the TiO_2 nanostructures followed by the adsorption of YFP. Reproduced from ref 28, copyright 2015 American Chemical Society.
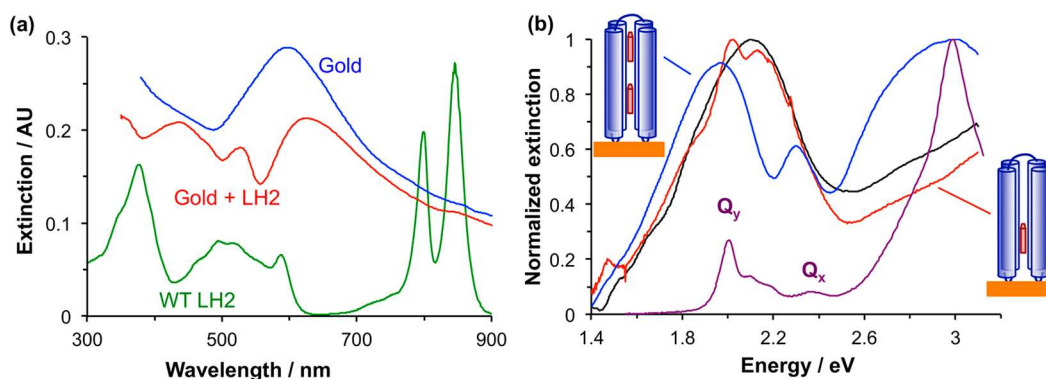
Figure 6. (a) Extinction spectrum of an array of gold nanostructures before (blue) and after (red) the attachment of His-tagged LH2. The absorption spectrum of the protein in the buffer is shown in green. Reproduced from ref 31. Copyright 2016 American Chemical Society. (b) Extinction spectrum of an array of gold nanostructures before (black) and after the attachment of one-chlorin maquettes (red) and two-chlorin maquettes (blue). Magenta: absorption spectrum of the two-chlorin maquette. (Both maquettes have identical absorption spectra.) Reproduced with permission from ref 40, copyright 2018 Royal Society of Chemistry.

resonance (LSPR) that combine the properties of light and matter. Wild-type and mutant LH1 and LH2 from *R. sphaeroides* containing different carotenoids yield different splitting energies, demonstrating that the coupling mechanism is sensitive to the electronic states in the light-harvesting complexes.

The coupling is a quantum optical phenomenon:[35] the plasmon mode is coupled to an array of emitters, and changes in the arrangement of excitons (for example, their density) lead to changes in the plasmon-exciton coupling energy and the energies of plexcitonic states. Thus, the strength of the coupling is expected to vary with the square root of the density of excitons in

the plasmon mode volume.[35] We modeled the system as coupled harmonic oscillators[36] and fitted the extinction spectra as a function of fractional coverage for His-tagged LH2 on gold nanostructure arrays. We found that the coupling energy E_C decreased with fractional coverage, confirming that the system was in the strong coupling regime.[31]

There has been a great deal of interest in the idea that quantum coherent excitations of multiple pigment molecules facilitate efficient energy transfer in light-harvesting complexes,[37,38] but the idea remains controversial. For example, Miller and co-workers recently argued that decoherence rates in
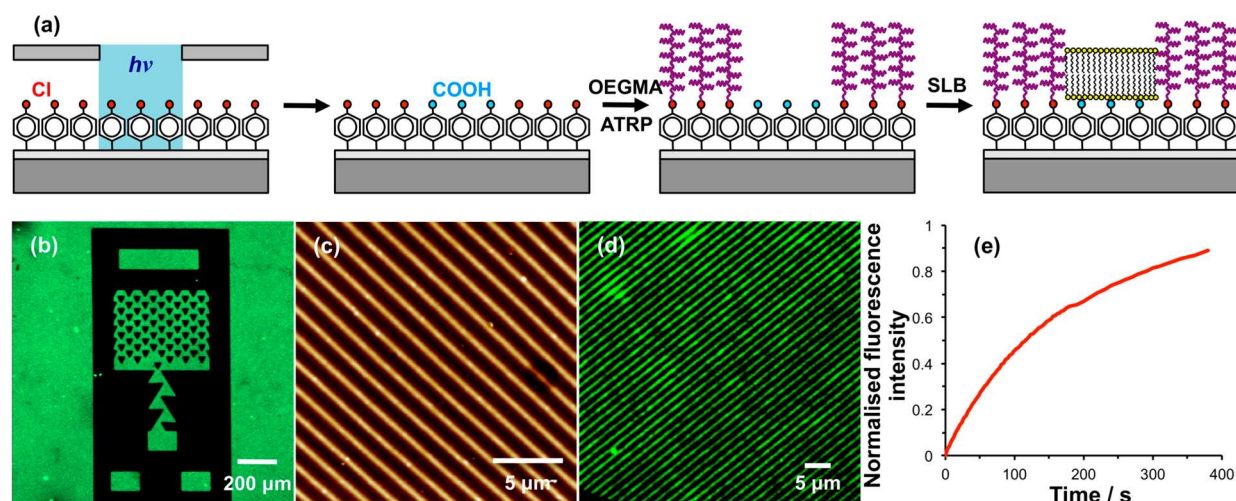
Figure 7. (a) Schematic diagram showing the fabrication of a patterned bilayer system.[43] (b) Fluorescence image showing SLB regions containing a low concentration of dye-labeled lipids (green) enclosed by POEGMA. (c) Nanochannels formed by IL. (d) Fluorescence image of SLBs in nanochannels. (e) Fluorescence recovery after photobleaching of lipids in nanochannels. Reproduced from ref 43, copyright 2017 American Chemical Society.

light-harvesting proteins are so fast under physiological conditions that electronic coherence could not contribute to photosynthesis.[39] However, while decisive evidence for quantum mechanical control of a biological process is lacking, we recently demonstrated for the first time that biological structures could be used to manipulate a quantum optical process.[40] In studies of synthetic light-harvesting maquette proteins with a single chlorin binding site, the plasmon mode was found to couple to an exciton with an energy of 2.06 ± 0.07 eV, close to the expected energy of the Q_y transition.[40] The coupling energy was 0.11 ± 0.01 eV, and a modest splitting of the plasmon band was observed in the extinction spectrum (Figure 6b). However, for maquettes containing two chlorin binding sites that are collinear in the field direction, an exciton energy of 2.20 ± 0.01 eV is obtained, intermediate between the energies of the Q_x and Q_y transitions of the chlorin. A much larger coupling energy of 0.27 ± 0.04 eV was determined from the modeling of the extinction spectrum, which exhibited a pronounced splitting of the plasmon band (Figure 6b). This observation is attributed to strong coupling of the LSPR to an H-dimer state not observed under weak coupling.

The interchromophore distance in the two-chlorin maquette is ~2 nm. At this separation, dipole coupling is weak and the FRET transfer rate is expected to be low. However, in strongly coupled systems, ultrafast exchange of energy occurs via the plasmon mode.[35] All of the emitters attached to a given nanoparticle (which may be as large as several hundred nanometers) are coherently coupled to the LSPR. Thus, the physics of strong coupling entails coherence over areas much larger than the dimensions of light-harvesting protein or the exciton diffusion lengths typical of molecular photonic materials. Because energy is exchanged via the plasmon mode and not through space, nonlocal couplings are possible, and we have found that they can be manipulated via control of the protein structure (e.g., replacement of pigment molecules to change exciton energies and transition dipole moments). The large increase in the coupling energy in the two-chlorin maquette compared to that in the one-chlorin maquette reflects the large transition dipole moment for the dimer state that is coupled to the plasmon mode.

These results are exciting because they suggest that molecular structures can be designed to manipulate strong plasmon–exciton coupling, thus enabling the design of structures that exhibit new optical properties. The incorporation of plasmonic nanostructures opens up new dimensions for the construction of low-dimensional systems, facilitating long-range energy exchange via plasmon-exciton coupling.

■ POLYMER BRUSHES ARE VERSATILE STRUCTURAL COMPONENTS IN THE DESIGN OF LOW-DIMENSIONAL SYSTEMS

We have used polymer brush synthesis by atom-transfer radical polymerization (ATRP)[41,42] as a means of fabricating structural and functional elements of low-dimensional systems. ATRP offers a simple, rapid means to grow dense grafted polymer films from solid substrates. It is a type of living radical polymerization: an initiator is attached to a surface, and the polymer is grown from this initiator with the initiator being transferred to the chain end as each monomer is added to the polymer. Commonly, a film of aminopropyl(triethoxy)silane (APTES) is formed on an oxide surface and derivatized by reaction with bromo-isobutyryl bromide (BIBB). Br yields fast polymer growth and well-controlled kinetics. However, Cl can also be used effectively as an initiator for ATRP. Films of chloromethyl-phenyltrichlorosilane (CMPTS) are readily patterned by exposure to UV light, leading to dehalogenation and the conversion of the chloromethyl group to a carboxylic acid. This proves to be a simple, effective method of patterning supported lipid bilayers.

Figure 7 shows a schematic diagram for the procedure used.[43] A film of CMPTS on a glass surface is exposed to UV light through a mask, leading to dehalogenation in exposed regions. In the masked areas, the chloromethyl groups remain intact, and poly(oligothylene glycol methacrylate) (POEGMA) brushes can be grown. POEGMA is resistant to lipids. Thus, when a supported lipid bilayer is formed on the sample by vesicle fusion, it avoids the POEGMA regions. Figure 7b shows a trap structure formed in this way. A small fraction of the lipids are labeled with the fluorescent dye Atto 488, enabling the SLB regions to be visualized by fluorescence microscopy. The dark features in Figure 7b correspond to regions that were masked during UV exposure; in these regions POEGMA has grown and has resisted

the formation of an SLB. The mobility of lipids in the exposed regions was determined to be 0.84 μm^2 s^{-1} using fluorescence recovery after photobleaching (FRAP), similar to values measured for SLBs supported on glass, and the mobile fraction was 98%.

Nanostructured SLBs can be fabricated by IL. Figure 7c shows an AFM image of channels that were designed with a period large enough (1.39 μm) to enable imaging by optical microscopy. The polymer-free regions (channels) in these structures had a width of ~300 nm. The fluorescence image in Figure 7d shows that after vesicle fusion the lipids are confined to the nanochannels. In FRAP measurements on these lipids (Figure 7e), a diffusion rate of 0.47 μm^2 s^{-1} was measured, which is within the normal range expected for mobile lipids on glass substrates although clearly slightly smaller than the value measured for the structure shown in Figure 7b.

An important design consideration when fabricating nanostructures from polymer brushes is that their structures and mechanical properties can be quite different from those of unpatterned films.[44−46] Photopatterning methods provide a simple and versatile method of exploring the dependence of the properties of low-dimensional brushes on their dimensions. Zhang et al. used near-field lithography to write lines of poly-(2-(methacryloyloxy)ethylphosphorylcholine) (PMPC) on a silicon surface functionalized by the adsorption of a film of nitrophenylpropyloxycarbonyl-protected APTES (NPPOC-APTES).[47] Exposure of the NPPOC-APTES film led to photodeprotection and exposure of the amine, which could be derivatized by reaction with BIBB to enable the growth of PMPC brushes by ATRP. By increasing the length of a series of lines monotonically while maintaining the same scan rate (frequency), it was possible to systematically control the dose rate, thus yielding a series of lines with systematically varying deprotection. The reaction between BIBB and the exposed amines is expected to be approximately quantitative, meaning that the resulting patterns yielded a systematically varying initiator density. It was found that the heights of the lines of surface-grafted polymers decreased smoothly as the writing rate was increased—there was not an abrupt transition from a brush to a mushroom conformation. The coefficients of friction of the lines (thought to be correlated with the degree of swelling of the brush[48]) also varied smoothly with the writing rate.

Al Jaf et al. addressed the same question by using UV light to modify brominated surfaces formed by the reaction of BIBB with APTES films.[49] On exposure to UV light, photolysis of the C−Br bond occurs. As the exposure is increased, the density of initiators at the surface is decreased, and consequently the density of a brush layer grown by ATRP is decreased. The relationship between the initiator density and the frictional properties of the brush layer was investigated by nanomechanical analysis of friction−load plots acquired for samples exposed to systematically varying UV doses. Using an approach that treats the friction force as the sum of load- and area-dependent terms, attributed respectively to energy dissipation in plowing and shearing, it is possible to fit friction−load plots and determine the surface shear strength τ of the polymer layer as a function of UV dose (Figure 8a). At low UV doses the value of τ increased with dose because the decreasing grafting density reduced the effective modulus of the brush layer, leading to an increase in the area of contact between the probe and the surface. However, τ reaches a maximum value at a dose of ~0.5 J cm^{-2}, and after this, it decreases, as the grafted polymers become less swollen and increasingly collapsed, causing more energy to be dissipated in plowing than through shearing.
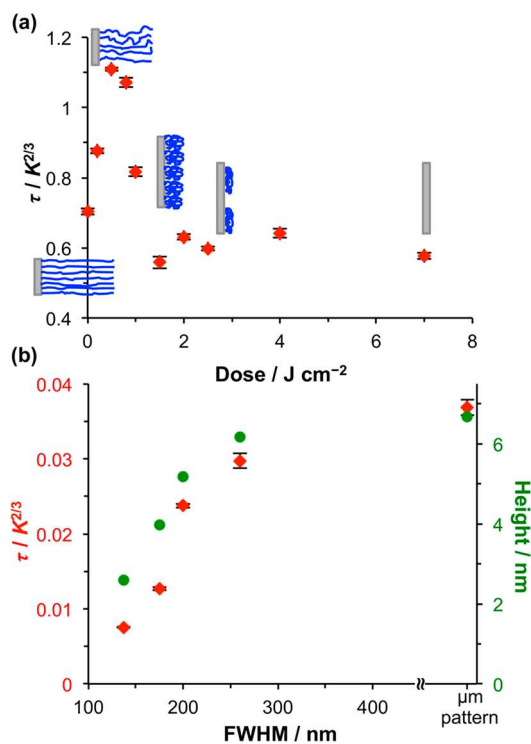
Figure 8. (a) Variation in the surface shear strength determined for poly(cysteine methacrylate) in water as a function of the UV dose. Schematic diagrams illustrate the change in polymer conformation with grafting density.[49] (b) Variation in the surface shear strength (diamonds) and height (circles) with feature size for brushes immersed in water. Reproduced with permission from ref 49, copyright 2017 Royal Society of Chemistry.

Nanostructured brushes were fabricated by using IL to selectively dehalogenate the surface. In regions exposed to intensity maxima, there is extensive modification of the surface, while in regions exposed to minima, there is negligible surface modification. Between these maxima and minima there was a gradient in Br density. Patterned Br-functionalized surfaces formed by IL were used to grow surface-grafted polymers by ATRP. For brushes grown under identical conditions, the height of the nanostructures was found to correlate with the pitch of the pattern—the larger the pitch, the higher the brush. As the fwhm increased from 137 to 260 nm, the height of poly(cysteine methacrylate) structures increased from 2.6 to 6.2 nm, approaching the unpatterned brush thickness of 6.7 nm (Figure 8b). This was attributed to a progressively decreasing lateral chain mobility as the feature size increases. Fully swollen brushes are observed only when a region forms at the center of the nanostructure in which the chain density is similar to that in an unpatterned film, and this limit is reached only as the brush width approaches 300 nm.

■ BINARY BRUSH SUPPORTS FOR LIPID BILAYERS

Poly(cysteine methacrylate) (PCysMA)[50,51] is a new poly-(amino acid methacrylate) that we have found to be a good support for lipid bilayers. The monomer is synthesized via thia-Michael addition of cysteine to a commercial methacrylate-acrylate precursor.[50] It can be prepared rapidly in multigram quantities in aqueous solution with minimal workup. PCysMA brush films can be grown from brominated surfaces by ATRP. These brushes are stimulus-responsive: at neutral pH they are zwitterionic, but below pH 3 they carry a net positive charge and
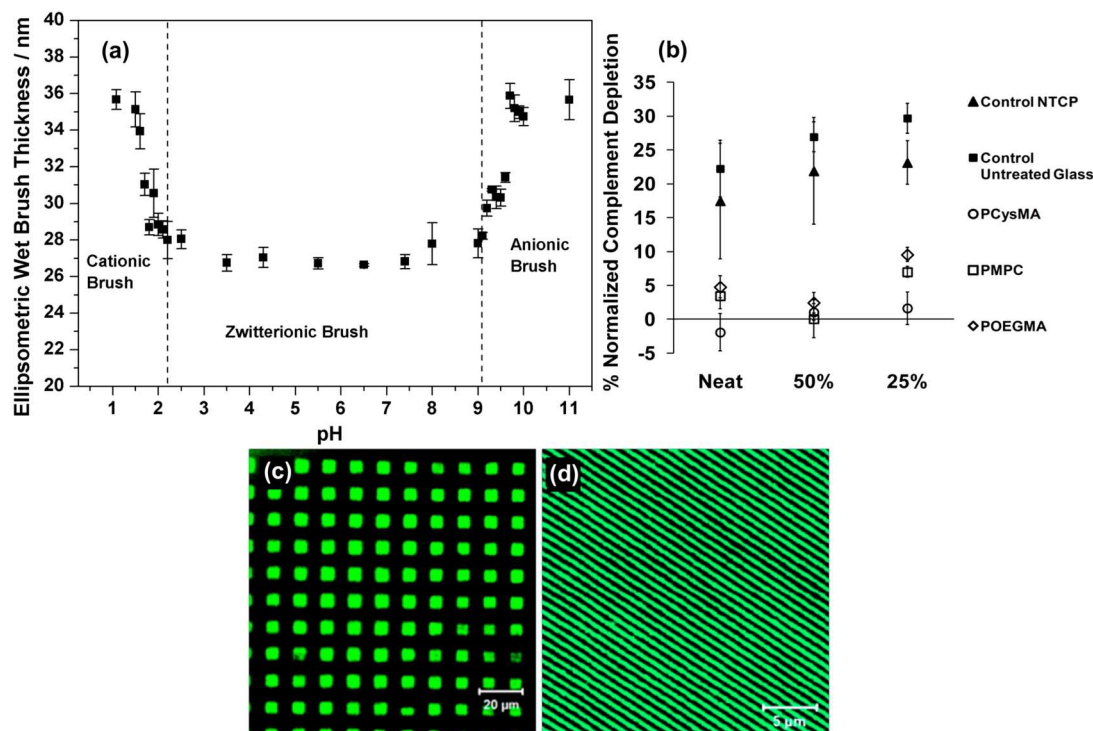
Figure 9. (a) Variation in the ellipsometric thickness of PCysMA brushes (dry thickness 15 nm). (b) Comparative complement depletion assays for three types of antibiofouling polymer brushes. PCysMA, PMPC, and POEGMA brushes of equivalent thickness (approximately 25−30 nm) were tested for complement depletion, and data were compared to both a nontissue culture (TC) plastic control (NTCP) and untreated glass. Antibiofouling performance was monitored over a range of human serum concentrations (100, 50, and 25%). (c) Micropatterns and (d) nanopatterns formed by UV exposure of PCysMA brushes followed by immersion in a solution of GFP. Reproduced from ref 50, copyright 2014 American Chemical Society.

above pH 9 they are negatively charged. Thus, at low and high pH there is additional swelling of the polymer brush by ∼30% (Figure 9a). PCysMA is exceptionally resistant to the adsorption of biological molecules and to the attachment of tissue cells. In studies of complement activation, it proved to be highly biologically inert, outperforming well-established antifouling polymer brushes POEGMA and PMPC (Figure 9b). However, exposure of PCysMA to UV light causes photodegradation, leading to the creation of protein-binding aldehyde functional groups. The brush can thus be patterned conveniently by mask-based exposure or by IL to enable the selective binding of proteins (Figure 9c,d).

Although PCysMA is biologically inert, it is an effective support for lipid bilayers.[52] Fusion of lipid vesicles containing 75% POPC (1-palmitoyl-2-oleoylphosphatidylcholine) and 25% DOTAP (1,2-dioleoyl-3-trimethylammonium-propane) yielded mobile lipid bilayers. Measurements of FRAP for SLBs formed from vesicles that contained a small amount of dye-labeled lipids indicated that the diffusion coefficient was 1.0 ± 0.02 m^2 s^{-1} and that the mobile fraction was 92%.

Good lipid mobilities were also measured for SLBs formed on poly(2-dimethylamino)ethyl methacrylate) (PDMA) brushes that had been quaternized by reaction with 1-iodooctadecane in *n*-hexane, which is a nonsolvent for PDMA.[53] Transfer of the brush to a nonsolvent causes the collapse of the polymer chains so that derivatization occurs only at the upper surface of the polymer film. On transfer to water, the derivatized polymer swells. In contrast, when the reaction is carried out in a good solvent for the polymer, tetrahydrofuran (THF), extensive quaternization occurs. Brushes that are derivatized in a poor solvent are pH-responsive because the majority of the amines

remain basic, while brushes prepared in a good solvent are not because the majority of the amines have been quaternized. Quaternization of PDMA brushes using 1-iodooctadecane in *n*-hexane provides the best protocol for the formation of robust SLBs: FRAP measurements on such SLBs indicate diffusion coefficients (2.8 ± 0.3 μm s^{-1}) and mobile fractions ($98 \pm 2\%$) comparable to the literature data reported for SLBs prepared directly on planar glass substrates.

A key design element in a low-dimensional system such as that shown in Figure 2c is the fabrication of "corrals" consisting of an SLB resting on a polymer brush cushion, surrounded by "walls" composed of a different polymer—a patterned binary brush structure. A number of workers have explored the fabrication of multicomponent polymer brushes using photopolymerization,[55] photolithography,[56−58] microcontact printing,[59,60] capillary force lithography,[61] and electron beam lithography.[46,62,63] Two-component brushes may also be formed by using complementary polymerization techniques.[64,65] Figure 10a shows schematically a route to such a structure based on photopatterning that is also compatible with nanofabrication using IL.[54] An NPPOC-APTES film is formed on a glass substrate and patterned to yield the selective deprotection of the adsorbates. In the exposed regions, a Br initiator is then attached to enable the growth of a polymer by ATRP. After the growth of this first polymer, the sample is flooded with near-UV light to cause the deprotection of adsorbates with intact protecting groups enabling the attachment of initiator to these regions that were masked during the initial UV patterning step. However, because ATRP is a living radical polymerization method, it is essential to remove the terminal Br atoms from the brushes grown in the first polymerization step before attempting the second polymerization.
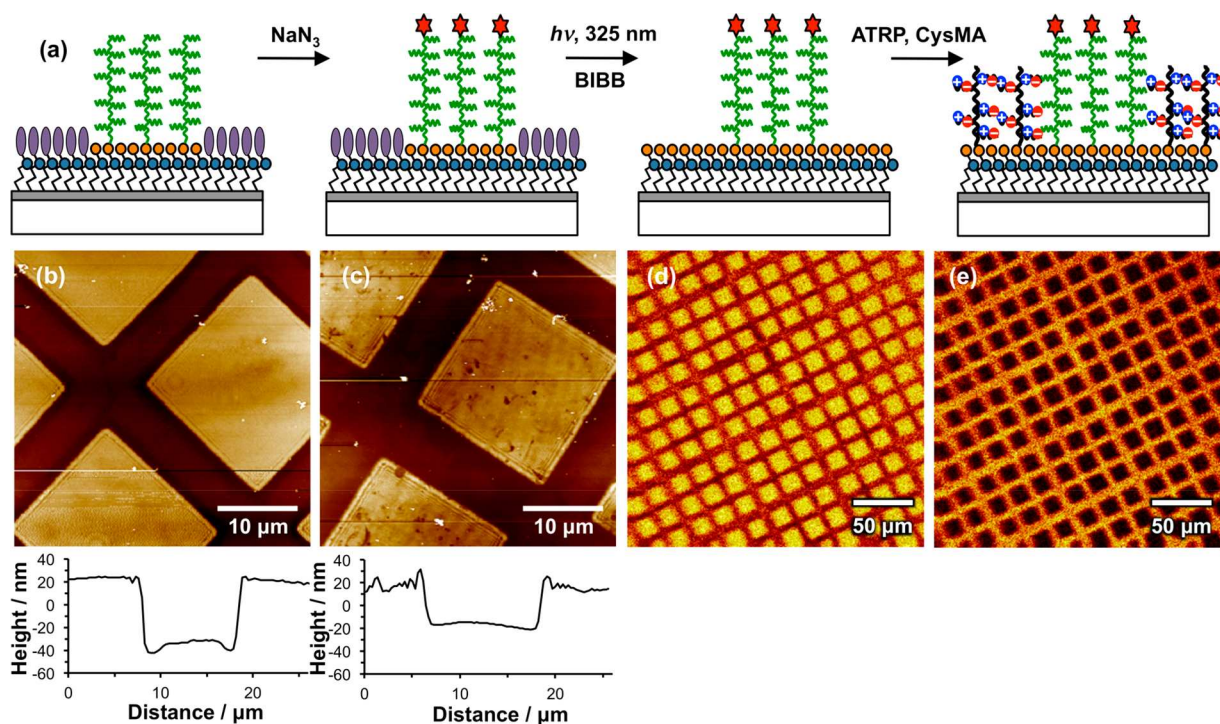
Figure 10. (a) Schematic diagram showing the formation of a binary brush structure by the photopatterning of NPPOC-APTES films combined with ATRP. (b) Tapping-mode topographical image of a micropatterned brush formed by UV photopatterning an NPPOC-APTES film followed by surface ATRP of OEGMEMA.[54] (c) Topographical image of the POEGMEMA brush sample shown in panel a following azide end-capping, UV exposure at 325 nm, BIBB treatment, and subsequent growth of PCysMA brushes via surface ATRP.[54] (d) SIMS image of the binary brush pattern obtained by mapping the summed intensities of the $C_2H_3O^-$ (m/z 43.04), $C_2H_2O_2^-$ (m/z 58.04), and $C_4H_5O_2^-$ (m/z 85.08) ions.[54] (e) Complementary SIMS image formed by mapping the summed intensities of the CN^- (m/z 26), S^- (m/z 32.07), HS^- (m/z 33.07), C_2HS^- (m/z 57.09), C_4HS^- (m/z 81.12), and $C_3H_5SO_2^-$ (m/z 105.12) ions. Reproduced with permission from ref 54, copyright 2017 Royal Society of Chemistry.

We find that this is conveniently achieved by the reaction of the brushes with sodium azide.[66] A minor complication with the use of NPPOC-APTES to fabricate binary brush structures is that there is a side reaction between BIBB and the carbamate bond in protected adsorbates that have not been exposed to UV light. This is addressed by adding a small amount of water to the BIBB to hydrolyze it, causing the formation of an anhydride, which does not attack the carbamate.

Figure 10b shows an AFM topographical image of a brush structure formed by exposing an NPPOC-APTES film to UV radiation through a 600 mesh copper grid, yielding patterned amine groups that were reacted with BIBB to yield a pattern of Br initiators from which POEGMEMA brushes were grown. The line section shows that the height difference between the masked and exposed regions was 54 nm after surface ATRP. The POEG-MEMA brush chain-ends were then azide-capped, and the wafer was irradiated at 325 nm to remove the remaining NPPOC groups, which enabled PCysMA brushes to be grown from these regions. The height difference between the square and the bar region of the pattern was reduced to 33 nm (Figure 10c), indicating the formation of a PCysMA brush with a mean thickness of 21 nm. SIMS imaging provided further evidence for the presence of two chemically distinct, spatially organized brushes within the pattern, with clear chemical contrast being observed and PCysMA-specific sulfur-containing ions being confined to the corrals (Figure 10d,e).

Corrals were formed in which PCysMA regions were enclosed by POEGMA (Figure 11a). SLBs were formed in the PCysMA regions by the fusion of vesicles containing a small amount of labeled lipids, enabling the structures to be imaged by
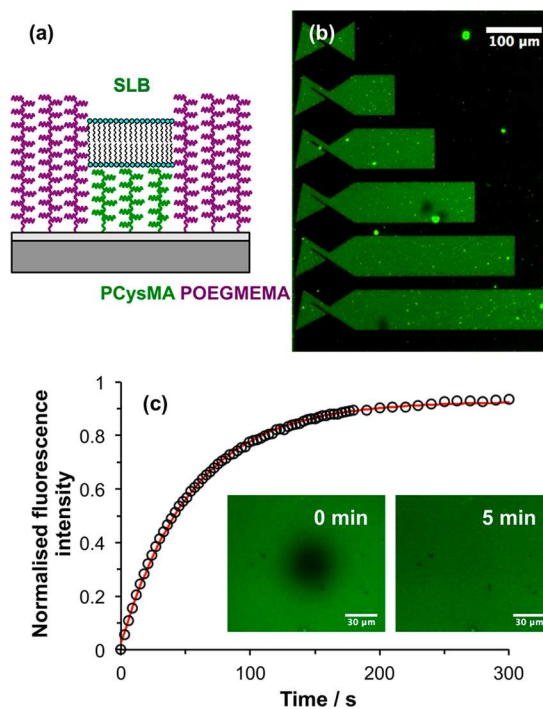
Figure 11. (a) PCysMA brush corral surrounded by POEGMEMA walls. (b) Fluorescence micrograph of a series of dc trap structures obtained after liposome adsorption and subsequent in situ rupture to form an SLB.[54] (c) Fluorescence recovery as a function of time after photobleaching. Circles: experimental data points. Red line: fitted recovery curve. Reproduced with permission from ref 54, copyright 2017 Royal Society of Chemistry.
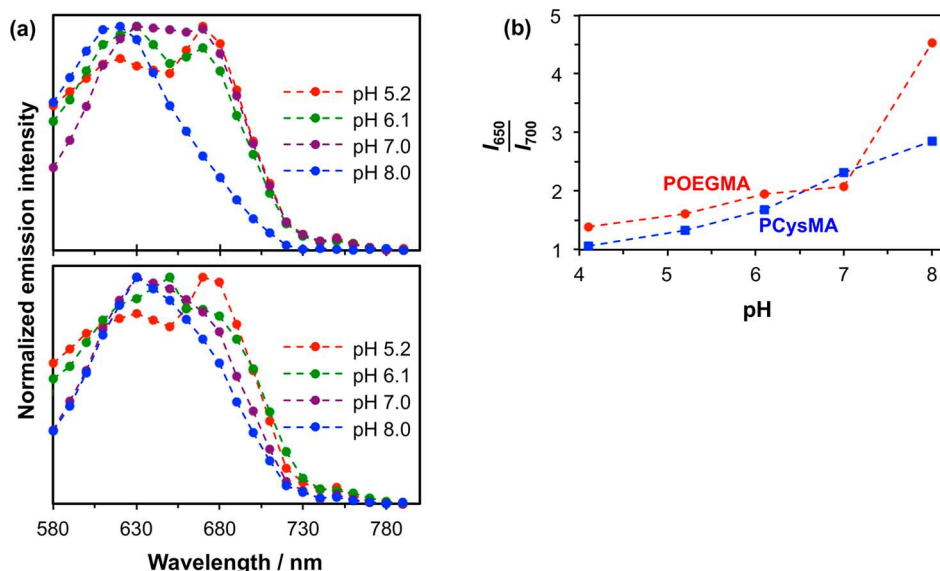
Figure 12. (a, Top) pH-dependent fluorescence spectra based on CLSM images of NBC-labeled POEGMA brushes (approximate dry brush thickness = 60 nm). (Bottom) pH-dependent fluorescence spectra based on CLSM images of NBC-labeled PCysMA brushes (approximate dry brush thickness = 10 nm). (b) Ratiometric fluorescence vs pH plot obtained for these PCysMA and POEGMA brushes. Reproduced with permission from ref 67, copyright 2018 Royal Society of Chemistry.

fluorescence microscopy (Figure 11b). Regions of bright contrast in the fluorescence image correspond to PCysMA regions on which an SLB has formed. These are surrounded by POEGMA, which exhibits dark contrast because it resists the formation of an SLB. FRAP measurements (Figure 11c,d) yield a mobile fraction of 93% and a diffusion coefficient of 1.36 $\mu m^2 \, s^{-1}$, comparable to literature values determined for the same lipids on positive control surfaces such as glass. These data provide strong evidence that the PCysMA corrals formed within POEG-MEMA walls enable the construction of spatially confined, highly mobile SLBs.

■ FUNCTIONAL MICROSYSTEM

The proton-motive force has a central importance in biology. For example, the function of the photosynthetic apparatus of *R. sphaeroides* shown in Figure 1 is to generate a proton gradient that will drive the conversion of ADP to ATP.[2] Thus, the design of low-dimensional systems that incorporate methods for the in situ measurement of proton concentration (via the pH) could be valuable for the modeling of many biological processes. The device shown in Figure 2c is a functional low-dimensional system that allows the measurement of transmembrane proton transport.[67] Rather than using the entire photosynthetic pathway depicted in Figure 1, proteorhodopsin (pR), a light-driven proton pump, is used. When illuminated, pR drives transmembrane proton transport. The pR is reconstituted into a lipid bilayer corral supported on a PCysMA cushion and enclosed within POEGMA walls. To facilitate pH measurement, a ratiometric dye is incorporated into the walls. Under illumination, pR pumps protons from the corral into the aqueous region above the membrane, raising the pH in the PCysMA cushion, which, in turn, causes the pH in the POEGMA walls to increase. Because the POEGMA is not capped by a lipid bilayer, the system is under kinetic control: a change in the local pH will be observed in the walls if the rate of proton transport across the lipid bilayer is greater than the rate of the diffusion of protons into the POEGMA from the aqueous medium above the corral.

To build binary brushes, a CMPTS film was photopatterned, causing the conversion of chloromethyl groups to carboxylic acids in exposed regions. The POEGMA walls were grown from chlorinated regions that had been masked during the patterning step. To enable pH measurement in the walls, POEGMA was polymerized in the presence of 0.1 equiv of Nile blue 2-(methacryloyloxy)ethyl carbamate (NBC) relative to copper(I). NBC is a methacrylate monomer that incorporates the pH-sensitive dye Nile blue. An additional property of this reagent is that the dye label acts as a radical spin trap: halogen end-groups are removed from the brushes via in situ dye addition upon transfer to the reaction mixture of 1 mol equiv of NBC relative to copper(I). The carboxylic acid groups can subsequently be derivatized to introduce a Br initiator, facilitating the growth of the second polymer (PCysMA) from regions that were exposed in the patterning step.

To calibrate the response of the NBC to pH changes, microstructured binary brushes were immersed in solutions of varying pH and characterized by microspectroscopy (thus enabling data to be collected from the two components of the binary brush structures separately). NBC was incorporated into both POEGMA and PCYSMA. For both polymers, a strong peak was observed at ca. 700 nm at a pH of 5.2 (Figure 12a), but at pH 8.0, the most intense peak in the spectrum was observed at ca. 650 nm. The ratio of the intensities at these wavelengths, I_{650}/I_{700}, was found to be diagnostic of the pH (Figure 12b).

To ensure the uniform orientation of pR at the PCysMA surface, a His-tagged mutant was used. PCysMA was first immersed in THF (a poor solvent for this polymer), causing the brushes to collapse and enabling the selective derivatization of carboxylate groups near the chain termini with NTA. After transfer to water and treatment with Ni^{2+}, the brushes bound His-tagged pR. The membrane was reconstituted by the fusion of vesicles that contained a small amount of Texas red-labeled lipid.[68] This enabled a qualitative evaluation of the efficacy of proton transport by pR. Figure 13b shows a confocal fluorescence image recorded for a POEGMA-NBC/PCysMA binary brush structure, where proteorhodopsin was first conjugated to
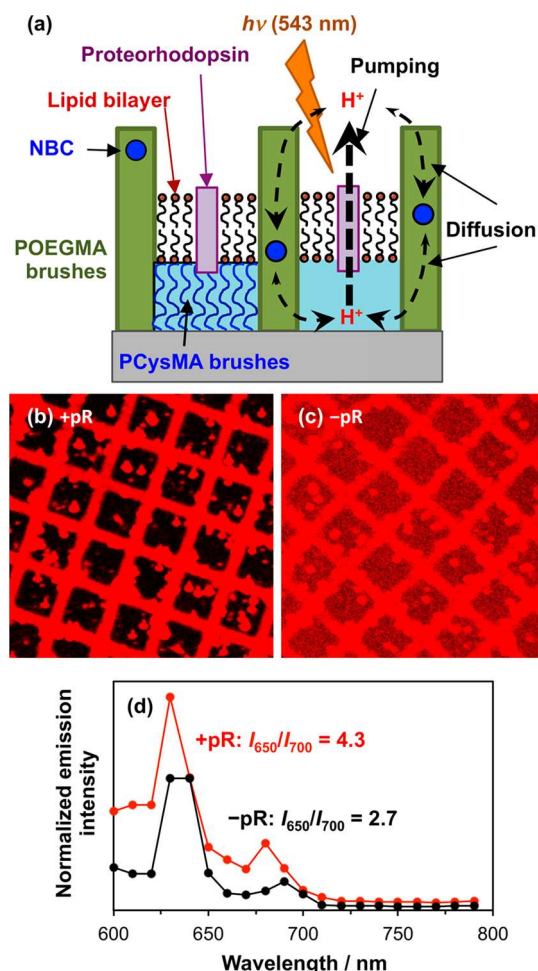
Figure 13. Proton pumping action of proteorhodopsin immobilized on a POEGMA-NBC/PCysMA binary brush structure.[67] (a) Schematic diagram of the model system. (b) Image formed by mapping the emission between 600 and 700 nm from POEGMA-NBC/PCysMA where pR is immobilized on PCysMA using a His tag, following bilayer formation. (c) Emission between 600 and 700 nm for POEGMA-NBC/PCysMA without pR following in situ bilayer formation by the addition of the lipid vesicle suspension. (d) Emission intensity from POEGMA-NBC walls for samples with and without immobilized pR. The I_{650}/I_{700} emission intensity ratio is calculated in each case and inserted with permission from ref 67, copyright 2018 Royal Society of Chemistry.

the PCysMA brush (square regions) followed by reconstitution of the protein into a lipid bilayer. The corrals exhibit dark contrast, but the walls containing Nile blue exhibit intense fluorescence. Fluorescence emission is increased under basic conditions; the bright fluorescence in Figure 13b is consistent with the maintenance of a basic pH in the walls. Figure 13c shows the corresponding binary brush system *without* proteorhodopsin. The contrast difference between the corrals and walls is now much smaller, and the low level of background emission from the labeled lipids (present at ~1% of the concentration of NBC in the lipid-resistant POEGMA brushes)[61] appears to be more significant.

These data indicate qualitatively that there is a significant difference in the local pH of the POEGMA walls depending on whether pR is present in the corrals. Ratiometric analysis based on the dependence of the I_{650}/I_{700} ratio on the pH allows the pH in the walls to be determined (Figure 13d). An I_{650}/I_{700} emission ratio of 4.3 was measured in the presence of proteorhodopsin, indicating a pH of ~8, whereas a I_{650}/I_{700} ratio of 2.7 in the

absence of proteorhodopsin suggests a pH of ~7.3 according to Figure 12b. At the very least, the significant difference in the emission ratio observed in the presence and absence of proteorhodopsin provides strong evidence for directional active proton pumping leading to the establishment of a changed local pH in the POEGMA walls.

This is a proof-of-concept experiment. However, it demonstrates the feasibility of constructing experimental systems using a combination of surface chemistry, photolithography, and ATRP that enable quantitative in situ monitoring of transmembrane transport. An important experimental challenge in the future will be to develop the system shown in Figure 13 to incorporate multiple different protein components. In order to replicate the organization found in biological membranes, these proteins should be organized within membranes on nanometer length scales. The system shown in Figure 13 relies upon the site-specific attachment of transmembrane proteins to a polymer brush; to achieve this in a spatially organized fashion, it would be necessary to control selectively the reactivity of the brush chain end to a protein-binding ligand. The tools to attempt this are effectively in place. Chapman et al. demonstrated the photo-patterning of polymer brushes using the selective deprotection of polymers end-capped using chloroformate derivatives of nitrophenylpropyloxycarbonyl protecting groups.[66] The fabrication of multiple-component nanostructures using near-field lithography of monolayers with nitrophenyl protecting groups has also been demonstrated.[21] Alternatively, interferometric lithography can be used to fabricate protein patterns with feature sizes commensurate with the distances over which spatial organization occurs in the chromatophore vesicle shown in Figure 1.[28]

Further challenges might include the design of functional nanosystems in which the corral size was reduced in size so that its surface area approached that of a single chromatophore vesicle, such as the one shown in Figure 1, and the integration of biosynthetic pathways, for example, by incorporating ATP synthase and measuring the rate of ATP production as a function of the architecture of the low-dimensional system.

■ CONCLUSIONS

There is an important sense in which, upon close inspection, all biological systems are low-dimensional. Cellular processes may best be viewed as sequences of single-molecule interactions. At the cellular level and below, the function of biological systems is profoundly different from that of binary, deterministic devices that are the basis of electronic technology: biological systems are intrinsically stochastic, utilizing gradients of composition to drive complex molecular processes occurring in fluid structures (proteins in cell membranes are in constant motion). Brownian processes (e.g., diffusion) are harnessed to transfer charge and signals in systems where the control of size is critical. The development of a detailed understanding of low-dimensional molecular systems can enhance our fundamental knowledge of how biological systems function and can also inspire the design of new kinds of devices and materials. While there has been an explosion of interest in systems biology in recent years, the development of experimental approaches to the study of biological systems has lagged far behind computational models. However, computational models must be tested experimentally. The system depicted schematically in Figure 13 provides a realistic empirical test bed against which the predictions of the computational analysis may be compared.

Although the fabrication of low-dimensional systems themselves presents substantial challenges for the experimentalist, the studies sketched in this Invited Feature Article provide a set of tools that may prove to be useful in designing systems for fundamental investigations. An obvious and significant extension of this work in the future would be to collaborate with computer scientists to begin integrating experimental outputs from low-dimensional systems with computer modeling. Huck has done this with impressive success for networks of interacting enzymatic reactions carried out in vesicles.[69]

The basic principles applied to light-driven processes in the examples discussed in this article should also be extendable to many other biological systems. The ubiquity of the proton-motive force in nature means that systems capable of the microscopic measurement of proton concentration will have widespread value in the study of biological systems. The importance of energy transfer in biology is of course far wider than photosynthesis; according to Schrödinger, living systems avoid the collapse into equilibrium by generating "negative entropy" through the action of the metabolism.[70] The development of experimental systems for the study of the transport of energy in biological systems would be important in many processes, for example, in understanding the function of the mitochondrion. While the structure shown in Figure 13 is a functional low-dimensional system, there are many ways that it could be elaborated, enabling a much wider set of biological problems to be explored.

■ AUTHOR INFORMATION

ORCID ⊙
Graham J. Leggett: 0000-0002-4315-9076

Notes
The author declares no competing financial interest.

Biography

Graham J. Leggett studied chemistry at the University of Manchester, completing his B.Sc. in 1987 and his Ph.D. in 1990. After postdoctoral research with Professor Buddy D. Ratner at the University of Washington and with Professor Martyn C. Davies at the University of Nottingham, he was appointed to a lectureship in materials at the University of Nottingham in 1994. In 1998, he returned to Manchester as a lecturer in physical chemistry, where he was promoted to senior lecturer and reader before taking up his current position in Sheffield in 2002. Currently he is Head of the Department of Chemistry. His research is focused on molecules and biomolecules at surfaces, and he is interested in both the modification of nanoscale surface structure (through the use of nanophotonic techniques) and also its characterization by quantitative scanning force microscopy techniques (such as friction force microscopy) and more recently by plasmonic techniques.

■ ACKNOWLEDGMENTS

■ REFERENCES

(1) Blankenship, R. E. *Molecular Mechanisms of Photosynthesis*, 2nd ed.; Wiley-Blackwell: Chichester, 2014; p 312.

(2) Cartron, M. L.; Olsen, J. D.; Sener, M.; Jackson, P. J.; Brindley, A. A.; Qian, P.; Dickman, M. J.; Leggett, G. J.; Schulten, K.; Neil Hunter, C. Integration of energy and electron transfer processes in the photosynthetic membrane of Rhodobacter sphaeroides. *Biochim. Biophys. Acta, Bioenerg.* **2014**, *1837*, 1769−1780.

(3) Kumar, S.; Cartron, M. L.; Mullin, N.; Qian, P.; Leggett, G. J.; Hunter, C. N.; Hobbs, J. K. Direct Imaging of Protein Organization in an Intact Bacterial Organelle Using High-Resolution Atomic Force Microscopy. *ACS Nano* **2017**, *11*, 126−133.

(4) Geyer, T.; Helms, V. Reconstruction of a kinetic model of the chromatophore vesicles from Rhodobacter sphaeroides. *Biophys. J.* **2006**, *91*, 927−937.

(5) Grayson, K. J.; Faries, K. M.; Huang, X.; Qian, P.; Dilbeck, P.; Martin, E. C.; Hitchcock, A.; Vasilev, C.; Yuen, J. M.; Niedzwiedzki, D. M.; Leggett, G. J.; Holten, D.; Kirmaier, C.; Neil Hunter, C. Augmenting light coverage for photosynthesis through YFP-enhanced charge separation at the Rhodobacter sphaeroides reaction centre. *Nat. Commun.* **2017**, *8*, 13972.

(6) Harris, J. M. *Poly(Ethylene Glycol) Chemistry: Biochemical and Biomedical Applications*; Plenum: New York, 1992.

(7) Prime, K. L.; Whitesides, G. M. Self-assembled organic monolayers: model systems for studying adsorption of proteins at surfaces. *Science* **1991**, *252*, 1164−1167.

(8) Pale-Grosdemange, C.; Simon, E. S.; Prime, K. L.; Whitesides, G. M. Formation of self-assembled monolayers by chemisorption of derivatives of oligo(ethylene glycol) of structure HS-$(CH_2)_{11}(OCH_2CH_2)_mOH$ on gold. *J. Am. Chem. Soc.* **1991**, *113*, 12−20.

(9) Lopez, G. P.; Albers, M. W.; Schreiber, S. L.; Carroll, R.; Peralta, E.; Whitesides, G. M. Convenient Methods for Patterning the Adhesion of Mammalian Cells to Surfaces using Self-Aseembled Monolayers of Alkanethiolates on Gold. *J. Am. Chem. Soc.* **1993**, *115*, 5877−5878.

(10) Ma, H.; Li, D.; Sheng, X.; Zhao, B.; Chilkoti, A. Protein resistant polymer brushes on silicon oxide by surface initiated atom transfer radical polymerization. *Langmuir* **2006**, *22*, 3751−3756.

(11) Hucknall, A.; Rangarajan, S.; Chilkoti, A. In Pursuit of Zero: Polymer Brushes that Resist the Adsorption of Proteins. *Adv. Mater.* **2009**, *21*, 2441−2446.

(12) Zhang, Z.; Chao, T.; Chen, S.; Jiang, S. Superlow Fouling Sulfobetaine and Carboxybetaine Polymers on Glass Slides. *Langmuir* **2006**, *22*, 10072−10077.

(13) Yang, W.; Chen, S.; Cheng, G.; Vaisocherová, H.; Xue, H.; Li, W.; Zhang, J.; Jiang, S. Film Thickness Dependence of Protein Adsorption from Blood Serum and Plasma onto Poly(sulfobetaine)-Grafted Surfaces. *Langmuir* **2008**, *24*, 9211−9214.

(14) Feng, W.; Zhu, S.; Ishihara, K.; Brash, J. L. Adsorption of Fibrinogen and Lysozyme on Silicon Grafted with Poly(2-methacryloyloxyethyl Phosphorylcholine) via Surface-Initiated Atom Transfer Radical Polymerization. *Langmuir* **2005**, *21*, 5980−5987.

(15) Feng, W.; Brash, J. L.; Zhu, S. Non-biofouling materials prepared by atom transfer radical polymerization grafting of 2-methacrylolox-

yethyl phosphorylcholine: Separate effects of graft density and chain length on protein repulsion. *Biomaterials* **2006**, *27*, 847−855.

(16) Fodor, S. P.; Read, J. L.; Pirrung, M. C.; Stryer, L.; Lu, A. T.; Solas, D. Light-directed, spatially addressable parallel chemical synthesis. *Science* **1991**, *251*, 767−773.

(17) Alang Ahmad, S. A.; Wong, L. S.; ul-Haq, E.; Hobbs, J. K.; Leggett, G. J.; Micklefield, J. Protein Micro- and Nanopatterning Using Aminosilanes with Protein-Resistant Photolabile Protecting Groups. *J. Am. Chem. Soc.* **2011**, *133*, 2749−2759.

(18) Xia, S.; Cartron, M.; Morby, J.; Bryant, D. A.; Hunter, C. N.; Leggett, G. J. Fabrication of Nanometer- and Micrometer-Scale Protein Structures by Site-Specific Immobilization of Histidine-Tagged Proteins to Aminosiloxane Films with Photoremovable Protein-Resistant Protecting Groups. *Langmuir* **2016**, *32*, 1818−1827.

(19) Reynolds, N. P.; Tucker, J. D.; Davison, P. A.; Timney, J. A.; Hunter, C. N.; Leggett, G. J. Site-Specific Immobilization and Micrometer and Nanometer Scale Photopatterning of Yellow Fluorescent Protein on Glass Surfaces. *J. Am. Chem. Soc.* **2009**, *131*, 896−897.

(20) Leggett, G. J. Light-directed nanosynthesis: near-field optical approaches to integration of the top-down and bottom-up fabrication paradigms. *Nanoscale* **2012**, *4*, 1840−1855.

(21) El Zubir, O.; Xia, S.; Ducker, R. E.; Wang, L.; Mullin, N.; Cartron, M. L.; Cadby, A. J.; Hobbs, J. K.; Hunter, C. N.; Leggett, G. J. From Monochrome to Technicolor: Simple Generic Approaches to Multicomponent Protein Nanopatterning Using Siloxanes with Photoremovable Protein-Resistant Protecting Groups. *Langmuir* **2017**, *33*, 8829−8837.

(22) Ul-Haq, E.; Patole, S.; Moxey, M.; Amstad, E.; Vasilev, C.; Hunter, C. N.; Leggett, G. J.; Spencer, N. D.; Williams, N. H. Photocatalytic Nanolithography of Self-Assembled Monolayers and Proteins. *ACS Nano* **2013**, *7*, 7610−7618.

(23) Christman, K. L.; Schopf, E.; Broyer, R. M.; Li, R. C.; Chen, Y.; Maynard, H. D. Positioning Multiple Proteins at the Nanoscale with Electron Beam Cross-Linked Functional Polymers. *J. Am. Chem. Soc.* **2009**, *131*, 521−527.

(24) Lau, U. Y.; Saxer, S. S.; Lee, J.; Bat, E.; Maynard, H. D. Direct Write Protein Patterns for Multiplexed Cytokine Detection from Live Cells Using Electron Beam Lithography. *ACS Nano* **2016**, *10*, 723−729.

(25) Haq, E. u.; Liu, Z.; Zhang, Y.; Ahmad, S. A. A.; Wong, L.-S.; Armes, S. P.; Hobbs, J. K.; Leggett, G. J.; Micklefield, J.; Roberts, C. J.; Weaver, J. M. R. Parallel Scanning Near-Field Photolithography: The Snomipede. *Nano Lett.* **2010**, *10*, 4375−4380.

(26) Brueck, S. R. J. Optical and Interferometric Lithography - Nanotechnology Enablers. *Proc. IEEE* **2005**, *93*, 1704−1721.

(27) Lu, C.; Lipson, R. H. Interference lithography: a powerful tool for fabricating periodic structures. *Laser Photon. Rev.* **2010**, *4*, 568−580.

(28) Moxey, M.; Johnson, A.; El-Zubir, O.; Cartron, M.; Dinachali, S. S.; Hunter, C. N.; Saifullah, M. S. M.; Chong, K. S. L.; Leggett, G. J. Fabrication of Self-Cleaning, Reusable Titania Templates for Nanometer and Micrometer Scale Protein Patterning. *ACS Nano* **2015**, *9*, 6262−6270.

(29) Tsargorodska, A.; El Zubir, O.; Darroch, B.; Cartron, M. l. L.; Basova, T.; Hunter, C. N.; Nabok, A. V.; Leggett, G. J. Fast, Simple, Combinatorial Routes to the Fabrication of Reusable, Plasmonically Active Gold Nanostructures by Interferometric Lithography of Self-Assembled Monolayers. *ACS Nano* **2014**, *8*, 7858−7869.

(30) Anker, J. N.; Hall, W. P.; Lyandres, O.; Shah, N. C.; Zhao, J.; Van Duyne, R. P. Biosensing with plasmonic nanosensors. *Nat. Mater.* **2008**, *7*, 442−453.

(31) Tsargorodska, A.; Cartron, M. L.; Vasilev, C.; Kodali, G.; Mass, O. A.; Baumberg, J. J.; Dutton, P. L.; Hunter, C. N.; Törmä, P.; Leggett, G. J. Strong Coupling of Localized Surface Plasmons to Excitons in Light-Harvesting Complexes. *Nano Lett.* **2016**, *16*, 6850−6856.

(32) Dintinger, J.; Klein, S.; Bustos, F.; Barnes, W. L.; Ebbesen, T. W. Strong coupling between surface plasmon-polaritons and organic molecules in subwavelength hole arrays. *Phys. Rev. B: Condens. Matter Mater. Phys.* **2005**, *71*, 035424.

(33) Shi, L.; Hakala, T. K.; Rekola, H. T.; Martikainen, J. P.; Moerland, R. J.; Törmä, P. Spatial Coherence Properties of Organic Molecules Coupled to Plasmonic Surface Lattice Resonances in the Weak and Strong Coupling Regimes. *Phys. Rev. Lett.* **2014**, *112*, 153002.

(34) Väkeväinen, A. I.; Moerland, R. J.; Rekola, H. T.; Eskelinen, A. P.; Martikainen, J. P.; Kim, D. H.; Törmä, P. Plasmonic Surface Lattice Resonances at the Strong Coupling Regime. *Nano Lett.* **2014**, *14*, 1721−1727.

(35) Törmä, P.; Barnes, W. L. Strong coupling between surface plasmon polaritons and emitters: a review. *Rep. Prog. Phys.* **2015**, *78*, 013901.

(36) Gallinet, B.; Martin, O. J. F. *Ab initio* theory of Fano resonances in plasmonic nanostructures and metamaterials. *Phys. Rev. B: Condens. Matter Mater. Phys.* **2011**, *83*, 235427.

(37) Lee, H.; Cheng, Y.-C.; Fleming, G. R. Coherence Dynamics in Photosynthesis: Protein Protection of Excitonic Coherence. *Science* **2007**, *316*, 1462−1465.

(38) Engel, G. S.; Calhoun, T. R.; Read, E. L.; Ahn, T.-K.; Mancal, T.; Cheng, Y.-C.; Blankenship, R. E.; Fleming, G. R. Evidence for wavelike energy transfer through quantum coherence in photosynthetic systems. *Nature* **2007**, *446*, 782−786.

(39) Duan, H.-G.; Prokhorenko, V. I.; Cogdell, R. J.; Ashraf, K.; Stevens, A. L.; Thorwart, M.; Miller, R. J. D. Nature does not rely on long-lived electronic quantum coherence for photosynthetic energy transfer. *Proc. Natl. Acad. Sci. U. S. A.* **2017**, *114*, 8493−8498.

(40) Lishchuk, A.; Kodali, G.; Mancini, J. A.; Broadbent, M.; Darroch, B.; Mass, O. A.; Nabok, A.; Dutton, P. L.; Hunter, C. N.; Törmä, P.; Leggett, G. J. A Synthetic Biological Quantum Optical System. *Nanoscale* **2018**, *10*, 13064−13073.

(41) Patten, T. E.; Matyjaszewski, K. Atom Transfer Radical Polymerization and the Synthesis of Polymeric Materials. *Adv. Mater.* **1998**, *10*, 901−915.

(42) Matyjaszewski, K.; Xia, J. Atom Transfer Radical Polymerization. *Chem. Rev.* **2001**, *101*, 2921−2990.

(43) Johnson, A.; Bao, P.; Hurley, C. R.; Cartron, M.; Evans, S. D.; Hunter, C. N.; Leggett, G. J. Simple, Direct Routes to Polymer Brush Traps and Nanostructures for Studies of Diffusional Transport in Supported Lipid Bilayers. *Langmuir* **2017**, *33*, 3672−3679.

(44) Kaholek, M.; Lee, W.-K.; LaMattina, B.; Caster, K. C.; Zauscher, S. Fabrication of Stimulus-Responsive Nanopatterned Polymer Brushes by Scanning Probe Lithography. *Nano Lett.* **2004**, *4*, 373−376.

(45) Kaholek, M.; Lee, W.-K.; Ahn, S.-J.; Ma, H.; Caster, K. C.; LaMattina, B.; Zauscher, S. Stimulus-Responsive Poly(N-isopropylacrylamide) Brushes and Nanopatterns Prepared by Surface-Initiated Polymerization. *Chem. Mater.* **2004**, *16*, 3688−3696.

(46) Lee, W.-K.; Patra, M.; Linse, P.; Zauscher, S. Scaling Behavior of Nanopatterned Polymer Brushes. *Small* **2007**, *3*, 63−66.

(47) Zhang, Z. J.; Moxey, M.; Alswieleh, A.; Armes, S. P.; Lewis, A. L.; Geoghegan, M.; Leggett, G. J. Nanotribological Investigation of Polymer Brushes with Lithographically Defined and Systematically Varying Grafting Densities. *Langmuir* **2017**, *33*, 706−713.

(48) Zhang, Z.; Morse, A. J.; Armes, S. P.; Lewis, A. L.; Geoghegan, M.; Leggett, G. J. Effect of Brush Thickness and Solvent Composition on the Friction Force Response of Poly(2-(methacryloyloxy)-ethylphosphorylcholine) Brushes. *Langmuir* **2011**, *27*, 2514−2521.

(49) Al-Jaf, O.; Alswieleh, A.; Armes, S. P.; Leggett, G. J. Nanotribological properties of nanostructured poly(cysteine methacrylate) brushes. *Soft Matter* **2017**, *13*, 2075−2084.

(50) Alswieleh, A. M.; Cheng, N.; Canton, I.; Ustbas, B.; Xue, X.; Ladmiral, V.; Xia, S.; Ducker, R. E.; El Zubir, O.; Cartron, M. L.; Hunter, C. N.; Leggett, G. J.; Armes, S. P. Zwitterionic Poly(amino acid methacrylate) Brushes. *J. Am. Chem. Soc.* **2014**, *136*, 9404−9413.

(51) Ladmiral, V.; Charlot, A.; Semsarilar, M.; Armes, S. P. Synthesis and characterization of poly(amino acid methacrylate)-stabilized diblock copolymer nano-objects. *Polym. Chem.* **2015**, *6*, 1805−1816.

(52) Blakeston, A. C.; Alswieleh, A. M.; Heath, G. R.; Roth, J. S.; Bao, P.; Cheng, N.; Armes, S. P.; Leggett, G. J.; Bushby, R. J.; Evans, S. D. New Poly(amino acid methacrylate) Brush Supports the Formation of Well-Defined Lipid Membranes. *Langmuir* **2015**, *31*, 3668−3677.

(53) Cheng, N.; Bao, P.; Evans, S. D.; Leggett, G. J.; Armes, S. P. Facile Formation of Highly Mobile Supported Lipid Bilayers on Surface-Quaternized pH-Responsive Polymer Brushes. *Macromolecules* **2015**, *48*, 3095−3103.

(54) Johnson, A.; Madsen, J.; Chapman, P.; Alswieleh, A.; Al Jaf, O.; Bao, P.; Hurley, C.; Cartron, M. L.; Evans, S.; Hobbs, J.; Hunter, N.; Armes, S. P.; Leggett, G. J. Micrometre and Nanometre Scale Patterning of Binary Polymer Brushes, Supported Lipid Bilayers and Proteins. *Chem. Sci.* **2017**, *8*, 4517−4526.

(55) Konradi, R.; Rühe, J. Fabrication of Chemically Microstructured Polymer Brushes. *Langmuir* **2006**, *22*, 8571−8575.

(56) Zhou, F.; Jiang, L.; Liu, W.; Xue, Q. Fabrication of Chemically Tethered Binary Polymer-Brush Pattern through Two-Step Surface-Initiated Atomic-Transfer Radical Polymerization. *Macromol. Rapid Commun.* **2004**, *25*, 1979−1983.

(57) Yom, J.; Lane, S. M.; Vaia, R. A. Multi-component hierarchically structured polymer brushes. *Soft Matter* **2012**, *8*, 12009−12016.

(58) Hoshi, Y.; Xu, Y.; Ober, C. K. Photo-cleavable anti-fouling polymer brushes: A simple and versatile platform for multicomponent protein patterning. *Polymer* **2013**, *54*, 1762−1767.

(59) Zhou, F.; Huck, W. T. S. Surface grafted polymer brushes as ideal building blocks for "smart" surfaces. *Phys. Chem. Chem. Phys.* **2006**, *8*, 3815−3823.

(60) Wei, Q.; Yu, B.; Wang, X.; Zhou, F. Stratified polymer brushes from microcontact printing of polydopamine initiator on polymer brush surfaces. *Macromol. Rapid Commun.* **2014**, *35*, 1046−1054.

(61) Liu, Y.; Klep, V.; Luzinov, I. To Patterned Binary Polymer Brushes via Capillary Force Lithography and Surface-Initiated Polymerization. *J. Am. Chem. Soc.* **2006**, *128*, 8106−8107.

(62) Paik, M. Y.; Xu, Y.; Rastogi, A.; Tanaka, M.; Yi, Y.; Ober, C. K. Patterning of Polymer Brushes. A Direct Approach to Complex, Sub-Surface Structures. *Nano Lett.* **2010**, *10*, 3873−3879.

(63) Kaholek, M.; Lee, W.-K.; Feng, J.; LaMattina, B.; Dyer, D. J.; Zauscher, S. Weak Polyelectrolyte Brush Arrays Fabricated by Combining Electron-Beam Lithography with Surface-Initiated Photopolymerization. *Chem. Mater.* **2006**, *18*, 3660−3664.

(64) Tria, M. C. R.; Advincula, R. C. Electropatterning of binary polymer brushes by surface-initiated RAFT and ATRP. *Macromol. Rapid Commun.* **2011**, *32*, 966−971.

(65) Xu, F. J.; Song, Y.; Cheng, Z. P.; Zhu, X. L.; Zhu, C. X.; Kang, E. T.; Neoh, K. G. Controlled micropatterning of a Si(100) surface by combined nitroxide-mediated and atom transfer radical polymerizations. *Macromolecules* **2005**, *38*, 6254−6258.

(66) Chapman, P.; Ducker, R. E.; Hurley, C. R.; Hobbs, J. K.; Leggett, G. J. Fabrication of Two-Component, Brush-on-Brush Topographical Microstructures by Combination of Atom-Transfer Radical Polymerization with Polymer End-Functionalization and Photopatterning. *Langmuir* **2015**, *31*, 5935−5944.

(67) Madsen, J.; Ducker, R. E.; Al Jaf, O.; Cartron, M. L.; Alswieleh, A. M.; Smith, C. H.; Hunter, C. N.; Armes, S. P.; Leggett, G. J. Fabrication of microstructured binary polymer brush "corrals" with integral pH sensing for studies of proton transport in model membrane systems. *Chem. Sci.* **2018**, *9*, 2238−2251.

(68) Smith, E. A.; Coym, J. W.; Cowell, S. M.; Tokimoto, T.; Hruby, V. J.; Yamamura, H. I.; Wirth, M. J. Lipid Bilayers on Polyacrylamide Brushes for Inclusion of Membrane Proteins. *Langmuir* **2005**, *21*, 9644−9650.

(69) Deng, N.-N.; Yelleswarapu, M.; Zheng, L.; Huck, W. T. S. Microfluidic Assembly of Monodisperse Vesosomes as Artificial Cell Models. *J. Am. Chem. Soc.* **2017**, *139*, 587−590.

(70) Schrodinger, E. *What is Life?*; Cambridge University Press: Cambridge, 1944.